

Can Conformally Invariant Modified Gravity Solve The Hubble Tension?

Tal Adi¹ and Ely D. Kovetz¹

¹*Department of Physics, Ben-Gurion University of the Negev, Be'er Sheva 84105, Israel*

The discrepancy between early-Universe and direct measurements of the Hubble constant, known as the Hubble tension, recently became a pressing subject in high precision cosmology. As a result, a large variety of theoretical models have been proposed to relieve this tension. In this work we analyze a conformally-invariant modified gravity (CIMG) model of an evolving gravitational constant due to the coupling of a scalar field to the Ricci scalar, which is theoretically advantageous as it has only one free parameter and its influence is concentrated around matter-radiation equality, as required for solutions to the Hubble tension based on increasing the sound horizon at recombination. Inspired by similar recent analyses of so-called early-dark-energy models, we constrain the CIMG model using a combination of early and late-Universe cosmological datasets. In addition to the *Planck* 2018 cosmic microwave background (CMB) anisotropies and weak lensing measurements, baryon acoustic oscillations and the Supernova H0 for the Equation of State datasets, we also use large-scale structure (LSS) datasets such as the Dark Energy Survey year 1 and the full-shape power spectrum likelihood from the Baryon Oscillation Spectroscopic Survey, including its recent analysis using effective field theory, to check the effect of the CIMG model on the (milder) S_8 tension between the CMB and LSS. We find that the CIMG model can slightly relax the Hubble tension, with $H_0 = 69.6 \pm 1.6$ km/s/Mpc at 95% CL, while barely affecting the S_8 tension. However, current data does not exhibit strong preference for CIMG over the standard cosmological model. Lastly, we show that the planned CMB-S4 experiment will have the sensitivity required to distinguish between the CIMG model and the more general class of models involving an evolving gravitational constant.

I. INTRODUCTION

The standard Λ cold-dark-matter (CDM) cosmological model has been tested by numerous probes and has provided a remarkable explanation for cosmological observations such as the cosmic microwave background (CMB) anisotropies and the baryon acoustic oscillations (BAO). However, despite the immense successes of the Λ CDM model, there has been a growing discrepancy between the measured values of the Hubble constant H_0 —the current expansion rate of the Universe—as inferred from early-Universe probes, which assume the Λ CDM model, and late-Universe probes, which do not assume such a model.

Most of the late-Universe measurements constrain the value of H_0 by applying the distance-ladder method [1]. This method uses parallax measurements to characterize nearby stars (e.g. Cepheid-variable stars, “tip of the red giant branch” stars, Miras, etc.), which are then used to calibrate the luminosity of nearby Type-Ia supernovae (SNe), allowing distant SNeIa to be used to estimate the Hubble flow. The Supernova H0 for the Equation of State (SH0ES) collaboration, which uses Cepheids, recently obtained $H_0 = 74.03 \pm 1.42$ km/s/Mpc [2]. Other distance-ladder measurements lead to other values, most of them in rough agreement with SH0ES.

The measurement of CMB anisotropies, assuming the Λ CDM model, allows an indirect inference of the Hubble constant. Inferring the angular size of the sound horizon and constraining the matter and baryon energy densities directly from the CMB temperature, polarization and lensing power spectra, allows the *Planck* 2018 collaboration to determine $H_0 = 67.36 \pm 0.54$ km/s/Mpc [3]. A similar early-Universe approach can be taken using a combination of measurements without including CMB

anisotropies: Big Bang nucleosynthesis (BBN); BAO; the FIRAS CMB global temperature and late-Universe measurement (e.g. galaxy-lensing based) of the matter density. The result of such analyses agrees quite precisely with that of the CMB [4]. The value of H_0 inferred from the CMB measurements is in 4.4σ tension with the value reported by SH0ES, and a similar discrepancy is present in the majority of the H_0 values inferred from other variations of early and late Universe measurements [4].

Various theoretical solutions were hitherto suggested to solve the H_0 discrepancy, which can crudely be divided into two approaches: pre-recombination and post-recombination solutions. A recent review of the Hubble tension [5] argued that the pre-recombination solutions are more likely to work, mainly due to the fact that post-recombination solutions affect only the inferred value of H_0 , while the combined data from BAO and local H_0 measurements implies that a reduction of the sound horizon at last scattering is required as well (see, however, Ref. [6]). In particular, it was argued that the critical epoch for achieving such reduction of the sound horizon takes place just prior to recombination. An increasing number of models aim to realize such solutions.

Recent analyses [7–11] of a popular subclass of these models, referred to as “early dark energy” (EDE) [12–20], showed that while they reduce the H_0 discrepancy, full cosmological concordance is not restored due to their tendency to increase the S_8 discrepancy between CMB and large-scale-structure observables, as described below.

In this work we focus on another model suggested to resolve the H_0 tension, based on a subclass of scalar-tensor theory. This modified gravity (MG) family of models [21–24], implemented by the coupling of a homogeneous scalar field to the Ricci scalar, acts to increase

Newton’s gravitational constant G_N prior to matter-radiation equality z_{eq} (that takes place just before recombination), which increases the Hubble parameter (i.e. the expansion rate) prior to recombination. The increase in $H(z)$ prior to recombination reduces the sound horizon r_s and increases the inferred value of H_0 . The scalar field, initially frozen at some initial value, subsequently decays to zero, lowering the value of G_N to its current value during post-recombination era. We emphasize that this “natural” occurrence is in contrast to what happens in EDE models, where a fine-tuned parameter z_c determines when the EDE component becomes dominant.

The MG model is parameterized by the initial value of the field ϕ_i and the coupling constant ξ . Together, these parameters determine the deviation in Newton’s constant $\Delta G_N \approx -\xi\phi_i^2/M_P^2$. We will focus here on a special case of a conformally-invariant (CI) MG model, for which $\xi \equiv -1/6$ is fixed. The CIMG model thus introduces only one additional parameter, ϕ_i , compared to Λ CDM (and two fewer than the popular EDE model).

Although it offers a more natural and simple realization of the solution to the H_0 discrepancy, the CIMG model exhibits most of the deficiencies manifested in the EDE models, however to a lower extent. In EDE models, some of the Λ CDM parameters shift significantly in order to preserve the fit to the CMB data, while the CIMG model tends to more delicate shifts of these parameters.

The increase in the Hubble parameter generally acts to slightly suppress the the growth of perturbations, for the modes within the sound horizon, during the period of enhanced expansion. In the EDE scenario this suppression forces a shift upward in $\Omega_c h^2$, so as to compensate for the loss of efficiency in the perturbations growth, while n_s shifts upwards due to the localized contribution of the EDE component to the expansion rate, as detailed in Ref. [7]. On the other hand, the increase in the gravitational strength, in the CIMG scenario, already acts to compensate for this loss and therefore allows a smaller shift in the value of $\Omega_c h^2$ [21, 22]. Furthermore, since the deviation in G_N under the CIMG model is not as localized in redshift-space as the dominant period of the EDE component, n_s also does not shift as much. Another impact of CIMG, due to the stronger gravitation, is the downwards shift of the matter density Ω_m which reduces significantly, compared to the EDE scenario.

The increases in $\Omega_c h^2$ and n_s increase the late-time amplitude of the density fluctuations σ_8 , aggravating the current (mild) tension between LSS and CMB inferences of this parameter. We follow the convention in Ref. [25] to quantify the parameter shifts and the associated LSS-CMB tension by the combination of the parameters defined as $S_8 \equiv \sigma_8(\Omega_m/0.3)^{0.5}$, where σ_8 is the RMS mass fluctuations in a 8Mpc/ h at $z = 0$. LSS experiments [26–29] place a combined constraint of $S_8 = 0.770^{+0.018}_{-0.016}$, which is in about 2.7σ tension with the *Planck* 2018 CMB result. The results of the analysis of the EDE model in Ref. [7], which considered joint CMB-LSS constraints, showed that the EDE model may increase the tension in

up to 35%, compared to the Λ CDM model. We will see that the effect on S_8 of the CIMG model is much weaker.

In this work we consider the constraints on the CIMG model from different data sets composed of CMB, LSS and H_0 measurements. We find that overall the one-parameter CIMG model exhibits similar properties to those of the three-parameter EDE model, only more moderate. It allows a smaller increase in the value of H_0 at the cost of much smaller increase in the value of S_8 . The CIMG model is not favorable to Λ CDM by *Planck* primary-CMB data alone, but the inclusion of CMB lensing + BAO + redshift-space distortions (RSD) + SNIa + SH0ES datasets results in a detectable CIMG component (i.e. a non-zero ϕ_i). When using the EFT-based LSS constraints we find an even more significant CIMG component which results in a better fit to SH0ES data without worsening the fits to CMB and LSS datasets, compared to Λ CDM.

We conclude with a simple Fisher analysis to forecast the constraints on the CIMG model from the planned CMB-S4 experiment. In particular we show that it will be able to constrain $\xi \sim -1/6$ to high accuracy, thus distinguishing the CIMG model from other MG models.

II. MODEL

The inference of H_0 from CMB measurement requires the determination of three parameters: the sound horizon r_s^* , the angular diameter distance D_A^* and the angular acoustic scale θ_s^* , where “*” denotes last-scattering. These are related by $\theta_s^* \equiv r_s^*/D_A^*$, which is measured by *Planck* 2018 to about 0.03% precision [3]. Thus, any modified evolution of $H(z)$ must accommodate the fixed ratio between r_s^* and D_A^* . The sound horizon at last-scattering

$$r_s^* = \int_{z_*}^{\infty} \frac{dz}{H(z)} c_s(z), \quad (1)$$

depends on the evolution of $H(z)$ prior to recombination, while the angular diameter distance

$$D_A^* = \int_0^{z_*} \frac{dz}{H(z)} \quad (2)$$

depends on its evolution post-recombination (and can be used to set H_0). Writing the expression for θ_s^* explicitly:

$$\theta_s^* = \frac{\int_{z_*}^{\infty} \frac{dz}{\sqrt{G_N(z)} \sqrt{\rho_{r,0}(1+z)^4 + \rho_{m,0}(1+z)^3 + \rho_{\phi}}} c_s(z)}{\int_0^{z_*} \frac{dz}{\sqrt{G_N(z)} \sqrt{\rho_{r,0}(1+z)^4 + \rho_{m,0}(1+z)^3 + \rho_{\Lambda}}}}, \quad (3)$$

it is easy to see how an increase in the value of G_N or an introduction of a new dominant contribution to the energy density budget (as EDE models suggest), prior to recombination, acts to reduce the sound horizon while increasing $H(z)$. The CIMG model introduces a scalar field with non-minimal-coupling (NMC), causing an upward

shift in the value of Newton's gravitational constant G_N prior to recombination. Around matter-radiation equality the field becomes dynamic and decays, reducing Newton's constant back to its fiducial value. The increase in the gravitational strength enhances the growth of $H(z)$ during this period, which in turn reduces r_s^* and raises the inferred value of H_0 . Naively speaking, a deviation of about 15% in the value of G_N (while keeping all the other parameters fixed and neglecting the additional energy component) is enough to reduce r_s^* by 7%, as was suggested in Ref. [5].

The MG model [30, 31] we consider is described by the action

$$S = \frac{1}{2} \int d^4x \sqrt{-g} \left[\frac{F(\phi)}{2} R + \partial_\mu \phi \partial^\mu \phi + \mathcal{L}_m \right], \quad (4)$$

where $F(\phi) \equiv M_P^2 \left(1 + \xi \frac{\phi^2}{M_P^2} \right)$ is the effective Planck mass (i.e. the NMC to the Ricci scalar R) and \mathcal{L}_m is the Lagrangian density describing the remaining contents of the Universe. The field ϕ is coupled to the Ricci scalar through a dimensionless coupling constant ξ , while in the special case of CIMG we fix $\xi = -1/6$, for which the action is invariant under conformal transformations [32] and the number of additional parameters to the Λ CDM model reduces from two (ξ and ϕ_i) to one. The dynamics of the field ϕ are determined by the equation of motion

$$\ddot{\phi} + 3H\dot{\phi} - \xi R\phi = 0. \quad (5)$$

We demand that $\xi < 0$, therefore as long as $R \ll H$, the field remains frozen at its initial value ϕ_i .

The evolution of the Ricci scalar can be derived from Einstein's equation

$$R_{\mu\nu} - \frac{1}{2}g_{\mu\nu}R = 8\pi G_N T_{\mu\nu}. \quad (6)$$

Since the trace of the stress-energy tensor $T_{\mu\nu}$ vanishes for radiation-like components and is equal to ρ_m for matter-like components, by taking the trace of Eq. (6) we find that $R \propto \rho_m$. Therefore, the Ricci scalar is practically zero—compared to H^2 —during the radiation-dominated (RD) era. Thus the non-minimally coupled field becomes dynamic only around matter-radiation equality when it acquires an effective mass $m_\phi^2 \sim \xi R \sim \xi H^2$. Then it begins to roll towards its minimum value, as shown in Fig. 1. From the Friedmann equation

$$3FH^2 = \rho + \frac{\dot{\phi}^2}{2} + \Lambda - 3\dot{F}H \equiv \rho + \rho_\phi, \quad (7)$$

we may associate the extra terms as the energy density of the field ϕ , so that the energy density of the field,

$$\rho_\phi = \frac{1}{2}\dot{\phi}^2 - 6\xi H\phi\dot{\phi} - 3\xi H^2\phi^2, \quad (8)$$

scales as $a^{-4.5}$ during the matter-dominated (MD) era, and thus dilutes faster than radiation.

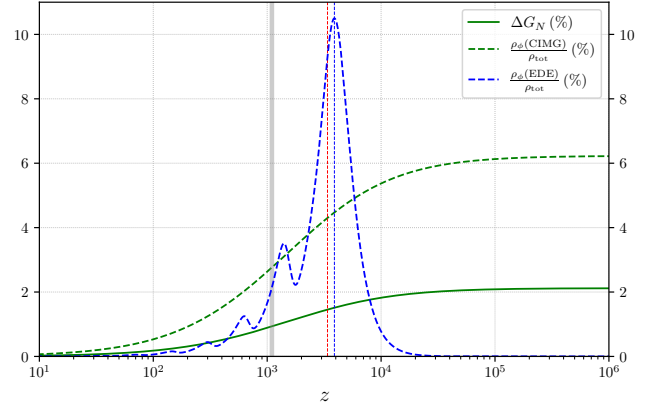


Figure 1. Evolution of the relative deviation of Newton's constant $\Delta G_N(\%) = 100 \times |G_N^*/G_N - 1|$ (solid green) and the energy fraction associated with ϕ (dashed green), in the CIMG scenario ($\xi = -1/6$), using the parameters specified in Table VII. For comparison, we also plot the energy fraction associated with the EDE field (dashed blue), corresponding to the best-fit values from Table IV in Ref. [7]. We also mark the matter-radiation equality (dashed red), the critical redshift of the EDE model (z_c parameter, vertical dashed blue), in which the EDE field is most dominant, and the recombination epoch (gray band). Both models become dynamic just prior to recombination (around matter-radiation equality). The EDE component is transiently dominant near z_c (peaks to over 10%), in contrast to the CIMG component which is present during the entire early-Universe era and is less significant (about 6%). The CIMG and EDE models were simulated by a modified version of hi-CLASS and the code of CLASS-EDE, respectively.

Because of the NMC, Newton's constant is replaced by an *effective Newton constant* $G_N^* \equiv (8\pi F)^{-1}$, and the deviation from General Relativity (GR) can be parameterized by $\Delta G_N \equiv |G_N^*/G_N - 1|$. The deviation from GR can also be parameterized by means of the so-called Post-Newtonian (PN) parameters [33]

$$\begin{aligned} \gamma_{PN} &= 1 - \frac{F_{,\phi}^2}{F + 2F_{,\phi}^2}, \\ \beta_{PN} &= 1 + \frac{FF_{,\phi}}{8F + 12F_{,\phi}^2} \frac{d\gamma_{PN}}{d\phi}, \end{aligned} \quad (9)$$

where the prediction from GR, i.e. $\gamma_{PN} = \beta_{PN} = 1$, is tightly constrained by Solar System experiments, as $\gamma_{PN} - 1 = (2.1 \pm 2.3) \times 10^{-5}$ and $\beta_{PN} - 1 = (4.1 \pm 7.8) \times 10^{-5}$ at 68% CL [34, 35]. Other studies of a varying cosmological constant place constraints on its value and its variation rate [36, 37]. Recent analysis, Ref. [21], showed that a deviation of about 2% in G_N at early times is enough to raise the Hubble constant to a value of $H_0 = 70.56$ km/s/Mpc, without conflicting with Solar System measurements.

III. METHODOLOGY AND DATASETS

We implement the CIMG model by modifying the public code for scalar-tensor theories `hi-class` [38, 39]¹, which in turn is based on the public Boltzmann code `CLASS` [40, 41]. In particular, we modified the Brans-Dicke model to match the CIMG model by replacing the Brans-Dicke related G_2 and G_4 functions with $G_2 = X - \Lambda$ and $G_4 = (1 + \xi\phi^2)/2$ (and $G_3 = G_5 = 0$), and their corresponding derivatives, where $X \equiv -\partial_\mu\phi\partial^\mu\phi/2$ and Λ plays the role of the cosmological constant.

We also added an extraction of $f\sigma_8(z)$ (taken from the public code `CLASS-EDE` [42]²), where $f \equiv d\log D/d\log a$ is the linear growth rate which is needed for implementing the RSD likelihoods in our analyses. In all likelihoods requiring calculations of the non-linear matter power spectrum, we used the “Halofit” prescription implemented in `CLASS`. We followed the analyses in [7], performing Markov-Chain-Monte-Carlo (MCMC) analyses, sampling the posterior distributions using the Metropolis-Hasting algorithm [43–45], implemented in the public code `Cobaya` [46]³, with Gelman-Rubin [47] convergence criteria $R - 1 < 0.05$. We used a uniform prior for the CIMG parameter $\phi_i = [0.005, 1]$ and Gaussian priors for the Λ CDM cosmological parameters, centered around the Λ CDM fiducial values. For the dataset combination which includes the EFT of LSS, we used `MontePython` [48, 49] for the MCMC analysis, along with the public code `PyBird` [9]⁴, which implements the EFT likelihood. We also used the public code `GetDist` [50]⁵ to analyze the MCMC chains: extract the best-fit parameters, mean values and errors, and plot the correlations in parameter-space as well as the maximized posteriors.

We used the same datasets used in Ref. [7], which include: *Planck* 2018 CMB temperature and polarization anisotropies power spectra (TT + TE + EE) and the CMB lensing (P18 and lensing) [3], Baryonic Acoustic Oscillations (BAO) [51–54], redshift-space distortion from SDSS BOSS DR12 (RSD) [51, 55], Type-Ia Supernovae (SNIa) [56], SH0ES 2019 H_0 measurements [2] and the Dark Energy Survey Year 1 (DES Y1) [26, 57], with the exception of additional LSS data from the Kilo-Degree Survey [27, 28] (KiDS) and the Hyper Suprime-Cam [29] (HSC) survey, which we used only as reference. We also included an additional dataset, comprising of the effective field theory (EFT) of LSS [9, 58–60] applied to the full shape power spectrum of the BOSS/SDSS galaxies clustering DR12 [61, 62] and the BAO post-reconstruction measurements from BOSS, combined with covariance between EFT-BOSS and anisotropic BAO

analysis. We did not use the south galactic cap (SGC) field of LOWZ, as in Ref. [59]. This dataset is henceforth referred to as BAO+EFT (not to be confused with the BAO dataset without EFT).

IV. RESULTS

We adopt the *Planck* convention, holding the sum of neutrino masses fixed to 0.06 eV, with one massive eigenstate against two massless eigenstates, and we fix the effective number of relativistic species to $N_{\text{eff}} = 3.046$. We also fit the Λ CDM model to each data set as a benchmark for comparison. A summary of the results is tabulated in Table IX.

A. CIMG Meets Primary CMB Alone

The first analysis we performed includes only the temperature and polarization anisotropies power-spectrum data from *Planck* 2018. While there is a small contribution to this dataset from LSS, due to gravitational lensing of the power spectra, the overall constraints are dominated by information from the recombination epoch. This analysis tests for evidence for the CIMG model using early-Universe data alone.

The results in Table I (see also Table IX) show very weak evidence for the CIMG model. The single CIMG parameter is constrained by an upper bound $\phi_i < 0.213 M_P$ (also indicated by the posterior shown in Fig. 4) and ΔG_N comprises 0 within 1σ . It seems that primary CMB data alone does not prefer the CIMG model over the standard Λ CDM model, and indeed the shift in the cosmological parameters is negligible (below 1σ of the Λ CDM benchmark). We also note that introducing an additional parameter beyond Λ CDM to the fit in the CIMG parameter model does not improve the fit as one might expect. On the contrary, we find $\Delta\chi^2 = +4.8$, as shown in Table II. We conclude that there is no preferred region, compared to the Λ CDM model, within the CIMG parameter space when considering the primary CMB data alone.

B. Expanding the analysis to also include CMB lensing, BAO, RSD, SNIa, and SH0ES

Following previous analyses [7, 13] of the EDE model, we include *Planck* 2018 CMB lensing, BAO, RSD, supernova, and local distance-ladder data in SH0ES 2019. This data set is considered a conclusive combination of early-Universe, LSS and SNeIa distance-ladder data.

We now find significant evidence for the CIMG model, with this combination of datasets. The initial value of the field, $\phi_i = 0.3^{+0.14}_{-0.24} M_P$ at 95% CL, and the fractional deviation of Newton’s constant, $\Delta G_N = 1.7 \pm 1.7$, both at 95% CL, are detected at $\geq 2\sigma$. As a result, the value of H_0 increases to $H_0 = 69.24 \pm 1.4$ km/s/Mpc,

¹ http://miguelzuma.github.io/hi_class_public/

² J. C. Hill, E. McDonough and M. W. Toomey: *Class-ed* https://github.com/mwt5345/class_ed

³ <https://cobaya.readthedocs.io/en/latest/>

⁴ <https://pybird.readthedocs.io/en/latest/>

⁵ <https://getdist.readthedocs.io/en/latest/>

Constraints on CIMG from *Planck* 2018 data only: TT+TE+EE

Parameter	Λ CDM	CIMG
$\log(10^{10} A_s)$	$3.044 (3.046) \pm 0.015$	$3.047 (3.035) \pm 0.016$
n_s	$0.9645 (0.9618) \pm 0.0042$	$0.9667 (0.9638)_{-0.0053}^{+0.0045}$
$100\theta_s$	$1.04185 (1.0419) \pm 0.00029$	$1.04189 (1.04151) \pm 0.00030$
$100 \times \Omega_b h^2$	$2.235 (2.23284) \pm 0.014$	$2.238 (2.23162) \pm 0.015$
$\Omega_c h^2$	$0.1202 (0.1210) \pm 0.0013$	$0.1200 (0.1206) \pm 0.0014$
τ_{reio}	$0.0540 (0.0547) \pm 0.0075$	$0.0547 (0.0489) \pm 0.0077$
$\phi_i [M_P]$	–	$< 0.213 (0.087)$
H_0 [km/s/Mpc]	$67.30 (66.98) \pm 0.58$	$67.98 (67.11)_{-1.1}^{+0.63}$
Ω_m	$0.3162 (0.3210) \pm 0.0081$	$0.310 (0.319)_{-0.0091}^{+0.012}$
σ_8	$0.8112 (0.8142) \pm 0.0072$	$0.8170 (0.8094)_{-0.020}^{+0.022}$
S_8	$0.833 (0.842) \pm 0.016$	$0.830 (0.834) \pm 0.016$
ΔG_N (%)	–	$0.68 (0.13)_{-0.75}^{+0.14}$

Table I. The mean (best-fit) $\pm 1\sigma$ (68% CL) constraints on the cosmological parameters in Λ CDM and CIMG as inferred from *Planck* 2018 primary CMB (TT+TE+EE) data alone. The CIMG component is not significant when considering early-Universe information (gravitational lensing have a little influence as well).

 χ^2 statistics from *Planck* 2018 data only: TT+TE+EE

Datasets	Λ CDM	CIMG
<i>Planck</i> 2018 low- ℓ TT	24.1	23.4
<i>Planck</i> 2018 low- ℓ EE	396.3	395.7
<i>Planck</i> 2018 high- ℓ TT+TE+EE	2345.1	2351.2
Total χ^2	2765.5	2770.3

Table II. χ^2 values for the best-fit Λ CDM and CIMG models, constrained by primary CMB alone. The additional parameter of the CIMG model does not improve the fit to the data as may be expected when increasing the total number of parameters.

compared to the Λ CDM benchmark, $H_0 = 68.17 \pm 0.77$ km/s/Mpc at 95% CL. The LSS likelihoods of RSD and BAO have large enough error bars to overlap with the region in parameter space with larger value of H_0 , reducing the Hubble tension to 3.1σ . This is due to both the increase in H_0 and its increased errors, emphasising the difficulty of reconciling all the likelihoods in the dataset.

In order to keep the fit with CMB and LSS data, other cosmological parameters shift as well. In particular $\Omega_c h^2$ and n_s shift upwards slightly, a 0.7σ and 0.4σ discrepancy with the benchmark, respectively. The degeneracy between H_0 and $\Omega_c h^2$ breaks due to the introduction of a new energy density component of the CIMG field, while its degeneracy with n_s increases (see Fig. 2). We also note a minuscule downward shift in $\Omega_b h^2$, 0.3σ discrepancy with the benchmark. In addition we find an increase in the value of σ_8 and a decrease in Ω_m , for which the net result is a minor increase in S_8 , which translates to a slightly larger tension with the combined LSS constraint: 2.4σ , compared to 2.2σ for the Λ CDM benchmark.

The CIMG component acts to increase the early-

Universe expansion rate, as $G_N^* > G_N$, thus suppressing the matter power spectrum $P(k)$ for modes within the sound horizon. This suppression requires an upward shift in $\Omega_c h^2$, which is the driver of the changes in $P(k)$, translated to a larger σ_8 . Moreover, as the enhanced expansion of the Universe is localized in time, the shift in the matter power spectra is scale dependent, affecting the value of n_s . Such behavior is expected, to some extent, for every model that acts to increase H_0 in such manner.

Compared to a recent analysis of the EDE model in Ref. [7], the CIMG model exhibits smaller shifts of the cosmological parameters (including H_0). Since the CIMG component is less localized in time, its free parameter ϕ_i is less correlated with n_s than the corresponding parameters in the EDE scenario. In addition, the enhanced gravitational strength acts to boost density anisotropies, which counteracts the need for increasing $\Omega_c h^2$. As a result, the matter density Ω_m is reduced, due to the increased Hubble parameter and the almost unchanged value of the CDM density. That is in contrast to the EDE model, which exhibits a significant increase in $\Omega_c h^2$ and no shift downwards in Ω_m , which results in a higher S_8 . Therefore the CIMG model offers to relax the H_0 tension, although not as much as the EDE model, but almost without worsening the CMB-LSS tension, when quantified in terms of the well-constrained S_8 parameter.

We find that the additional CIMG parameter improves the total fit to the data, with $\Delta\chi^2 = -9$, relative to the Λ CDM benchmark, as shown in Table IV. The reduction in χ^2 is mainly due to the better fit to the SH0ES likelihood which compensates for the degraded fit to the CMB datasets, while the fit to LSS data worsens only slightly, indicating the intrinsic tension between the datasets.

The different shifts in H_0 and S_8 values indicate stronger correlation of the EDE component f_{EDE} with H_0 and σ_8 than that of the CIMG parameter ϕ_i shown

Constraints from *Planck* 2018 TT+TE+EE + CMB Lensing,
BAO, RSD, SNIa and SH0ES

Parameter	Λ CDM	CIMG
$\log(10^{10} A_s)$	$3.051 (3.054)^{+0.013}_{-0.015}$	$3.051 (3.060) \pm 0.014$
n_s	$0.9689 (0.9691) \pm 0.0035$	$0.9711 (0.9727) \pm 0.0038$
$100\theta_s$	$1.04204 (1.04187) \pm 0.00027$	$1.04199 (1.04212) \pm 0.00028$
$100 \times \Omega_b h^2$	$2.253 (2.253) \pm 0.013$	$2.247 (2.24705) \pm 0.013$
$\Omega_c h^2$	$0.1183 (0.1185) \pm 0.0009$	$0.1193 (0.1192)^{+0.0010}_{-0.0011}$
τ_{reio}	$0.0593 (0.0618)^{+0.0065}_{-0.0075}$	$0.0565 (0.0601) \pm 0.0073$
$\phi_i [M_P]$	–	$0.297 (0.297)^{+0.11}_{-0.075}$
H_0 [km/s/Mpc]	$68.17 (68.07) \pm 0.39$	$69.24 (69.15)^{+0.60}_{-0.83}$
Ω_m	$0.3045 (0.3057) \pm 0.0051$	$0.297 (0.298)^{+0.007}_{-0.006}$
σ_8	$0.8088 (0.8103) \pm 0.0059$	$0.8242 (0.8267)^{+0.009}_{-0.012}$
S_8	$0.815 (0.818) \pm 0.010$	$0.820 (0.823) \pm 0.010$
ΔG_N (%)	–	$1.70 (1.49)^{+0.81}_{-1.1}$

Table III. The mean (best-fit) $\pm 1\sigma$ (68% CL) constraints on the cosmological parameters in the Λ CDM and CIMG scenarios, as inferred from the combination of P18 + lensing + BAO + SNIa + RSD + SH0ES datasets. There is significant evidence for the CIMG model as $\phi_i = 0.3^{+0.14}_{-0.24} M_P$ and $\Delta G_N = 1.7 \pm 1.7$ with 95% CL are detected at $\geq 2\sigma$ significance.

χ^2 statistics from the fit to *Planck* 2018 TT+TE+EE +
CMB Lensing, BAO, RSD, SNIa and SH0ES

Datasets	Λ CDM	CIMG
CMB TT, EE, TE:		
<i>Planck</i> 2018 low- ℓ TT	22.9	22.4
<i>Planck</i> 2018 low- ℓ EE	398.0	397.3
<i>Planck</i> 2018 high- ℓ TT+TE+EE	2350.9	2347.2
LSS:		
<i>Planck</i> CMB lensing	8.7	9.1
BAO (6dF)	0.002	0.035
BAO (DR7 MGS)	1.6	2.3
BAO+RSD (DR12 BOSS)	6.0	6.7
Supernovae:		
Pantheon	1034.8	1034.7
SH0ES	20.2	14.4
Total χ^2	3843.1	3834.1

Table IV. χ^2 values for the best-fit Λ CDM and CIMG models, constrained by P18 + lensing + BAO + RSD + SNIa + SH0ES datasets. There is reduction of 9 in the value of χ^2 , for the one additional CIMG parameter to Λ CDM, driven almost entirely by the improved fit to SH0ES. However, it is notable that the fit to the LSS data is worse in the CIMG scenario, while the fit to the CMB is not degraded.

in Fig. 4. Placing the CIMG model somewhere between Λ CDM and EDE in context of both H_0 and S_8 tensions.

C. Considering additional LSS data

We now expand our analysis to include likelihoods from the DES-Y1 dataset [26, 57], in particular the “3x2pt” likelihood, comprised of photometric galaxy clustering, galaxy-galaxy lensing, and cosmic shear two-point correlation functions.

The inclusion of DES data places stronger constraints on Ω_m , which in turn reduces the value of the CIMG parameter ϕ_i , as shown in Table V (see also Table IX). We find $\phi_i = 0.26^{+0.17}_{-0.23} M_P$ at 95% CL, detected with $\leq 2\sigma$ significance. Meanwhile, the value of H_0 shifts further upwards to $H_0 = 69.4^{+1.3}_{-1.2}$ km/s/Mpc at 95% CL. The reason for that is due to the general shift in H_0 when including the DES-Y1 dataset, observed also for the Λ CDM benchmark compared to Table III. Thus the tension with SH0ES measurements is reduced to 3σ for CIMG, compared to 3.8σ in the Λ CDM benchmark scenario.

The lower value of ϕ_i when DES-Y1 data is included in the combined dataset can be understood in terms of the interplay between σ_8 , Ω_m , H_0 and ϕ_i . The precise DES measurement of Ω_m breaks the $\Omega_m - H_0$ degeneracy in the Λ CDM fit to the CMB, shifting H_0 to larger values. The impact of the DES measurements on the CIMG parameter results in a lower value for ϕ_i , due to a marked correlation between σ_8 , H_0 and ϕ_i , observed in Fig. 4. The same thing happens in the EDE scenario with f_{EDE} replacing ϕ_i , only to greater extent due to its stronger degeneracy with σ_8 and H_0 .

It is also notable that the posterior of σ_8 matches closely that of the fit to primary CMB-only, as shown in Fig. 4, erasing the shift observed without DES. This shift manifests the constraints of LSS on ϕ_i , due to the correlation between σ_8 and ϕ_i , mentioned previously. The

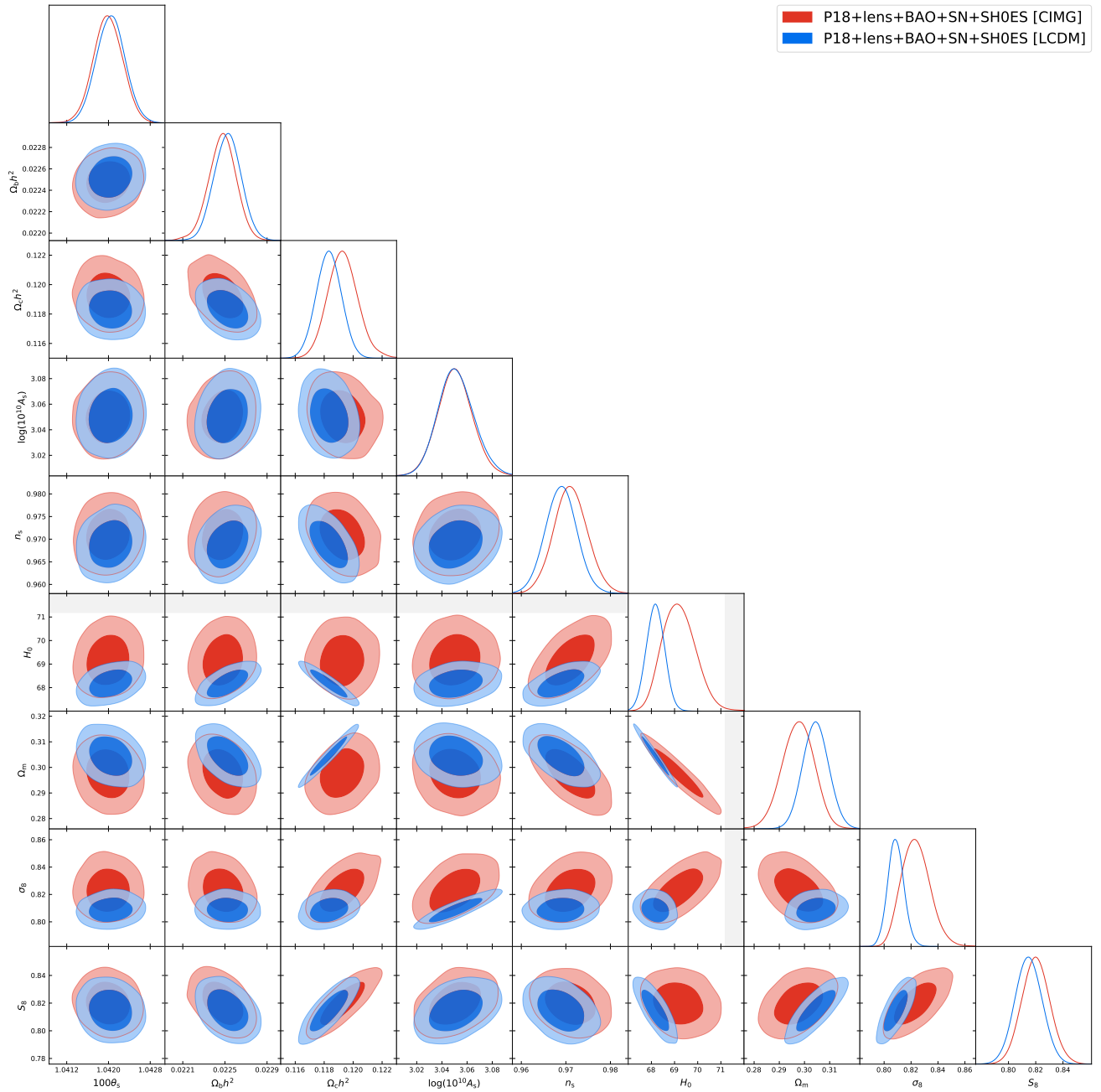


Figure 2. Cosmological parameter constraints from the combination of *Planck* 2018 primary CMB data (TT+TE+EE); *Planck* 2018 CMB lensing data; BAO data from 6dF, SDSS DR7, and SDSS DR12; Pantheon SNIa data; the latest SH0ES H_0 constraint; and SDSS DR12 RSD data. We do not plot τ , as it is essentially unchanged in the CIMG fit. Some parameters shift by a non-negligible amount in the CIMG fit (compared to Λ CDM), including increases in $\Omega_c h^2$, n_s , and σ_8 as well as broadening of the error bars on these parameters. The increase in H_0 is not large enough to reconcile the tension with the SH0ES-only constraint (shown in the grey bands), but it does reduce the tension significantly.

shift in σ_8 is matched by the shift in $S_8 = 0.809 \pm 0.018$ at 95% CL, which is in 1.9σ tension with combined LSS measurements, negligibly larger than the 1.8σ for Λ CDM.

The χ^2 statistics, tabulated in Table VI, show poor improvement to the fit for the additional CIMG parameter. The CIMG model offers a slightly better fit to SH0ES

data alone, compared to the Λ CDM benchmark, while the fit to LSS data worsens. It seems that there is no region in parameter space that is in concordance with all cosmological data sets. This indicates a possible statistical tension between LSS and H_0 likelihoods, as each dataset pulls the parameters in the opposite direction.

Constraints from *Planck* 2018 TT+TE+EE + CMB Lensing,
BAO, RSD, SNIa, SH0ES and DES-Y1

Parameter	Λ CDM	CIMG
$\log(10^{10} A_s)$	$3.049 (3.043) \pm 0.012$	$3.048 (3.053) \pm 0.014$
n_s	$0.9705 (0.9701) \pm 0.0030$	$0.9722 (0.9728) \pm 0.0037$
$100\theta_s$	$1.04208 (1.04183) \pm 0.00023$	$1.04205 (1.04179) \pm 0.00028$
$100 \times \Omega_b h^2$	$2.259 (2.258) \pm 0.011$	$2.255 (2.250) \pm 0.013$
$\Omega_c h^2$	$0.1176 (0.1179) \pm 0.0007$	$0.1183 (0.1184) \pm 0.0009$
τ_{reio}	$0.0591 (0.0544) \pm 0.0060$	$0.0569 (0.0563) \pm 0.0072$
$\phi_i [M_P]$	–	$0.264 (0.308)^{+0.13}_{-0.072}$
H_0 [km/s/Mpc]	$68.52 (68.30) \pm 0.30$	$69.40 (69.43)^{+0.60}_{-0.75}$
Ω_m	$0.2999 (0.3025) \pm 0.0039$	$0.2939 (0.2937) \pm 0.0058$
σ_8	$0.8056 (0.8038) \pm 0.0047$	$0.8176 (0.8216)^{+0.0087}_{-0.0110}$
S_8	$0.805 (0.807) \pm 0.007$	$0.809 (0.813) \pm 0.009$
ΔG_N (%)	–	$1.36 (1.61)^{+0.68}_{-1.1}$

Table V. The mean $\pm 1\sigma$ (68% CL) constraints on the cosmological parameters in Λ CDM and CIMG, as inferred from the combination of P18 + lensing + BAO + RSD + SNIa + SH0ES + DES-Y1. With the inclusion of DES data the evidence for CIMG decreases, as $\phi_i = 0.26^{+0.17}_{-0.23} M_P$ and $\Delta G_N = 1.4^{+1.7}_{-1.5}$ with 95% CL, to $\lesssim 2\sigma$ significance.

χ^2 statistics from the fit to *Planck* 2018 TT+TE+EE +
CMB Lensing, BAO, RSD, SNIa, SH0ES and DES-Y1

Datasets	Λ CDM	CIMG
CMB TT, EE, TE:		
<i>Planck</i> 2018 low- ℓ TT	22.4	22.3
<i>Planck</i> 2018 low- ℓ EE	396.0	396.3
<i>Planck</i> 2018 high- ℓ TT+TE+EE	2350.6	2350.5
LSS:		
<i>Planck</i> CMB lensing	9.4	9.2
BAO (6dF)	0.002	0.084
BAO (DR7 MGS)	1.9	2.7
BAO+RSD (DR12 BOSS)	5.8	7.3
DES-Y1	510.8	513.6
Supernovae:		
Pantheon	1034.8	1034.8
SH0ES	18.8	13.0
Total χ^2	4350.5	4349.7

Table VI. χ^2 values for the best-fit Λ CDM and CIMG models, constrained by CMB + lensing + BAO + RSD + SNIa + SH0ES + DES-Y1 datasets. There is reduction of only 0.8 in χ^2 , for the one additional parameter of the CIMG model.

We also test the CIMG model with another LSS dataset, using effective field theory (EFT) applied to BOSS DR12. this dataset is composed of *Planck* 2018 CMB + lensing + EFT with BAO + SH0ES. The results are tabulated in Table VII (and summarized in Table IX). The EFT dataset is less constraining, compared to DES-Y1, as it allows the largest CIMG component

of $\phi_i = 0.33^{+0.16}_{-0.20} M_P$ at 95% CL, which corresponds to a 2% relative deviation in ΔG_N . The CIMG component now raises the Hubble parameter to the value of $H_0 = 69.6 \pm 1.6$ km/s/Mpc at 95% CL, which is the most significant increase in H_0 , compared to the corresponding Λ CDM benchmark, of all the datasets tested in this work. The Hubble tension reduces, in this scenario, to 2.7σ , compared to 3.9σ for the Λ CDM benchmark. Again, the increase comes at the cost of upward shift of σ_8 . But the greater reduction in Ω_m results in a mild increase of S_8 , increasing the tension with the combined LSS constraints to just 2.3σ , compared to 2.1σ for Λ CDM.

The χ^2 statistics, shown in Table VIII, indicate a reduction of 6.5 in the total χ^2 value, compared to Λ CDM. This reduction is once again mainly due to SH0ES, but we also find a reduction in the χ^2 for some of the LSS likelihoods, resulting in a total increase of only 0.5 due to LSS fits, while the fit to CMB is practically not degraded.

This combination of datasets seems to provide a significant relaxation of the Hubble tension without a substantial damage to the fit to CMB and the LSS data, or a notable increase of the tension between these datasets, represented here by S_8 .

V. FORECAST FOR CMB-S4 CONSTRAINTS

In this work we analyzed the CIMG model, which is a special case of a MG model with a scalar field coupled to the Ricci scalar (i.e. fixing $\xi = -1/6$), because it is symmetric and involves only one additional parameter. Previous analysis of the more general model [21] (with ξ free to vary) has found that $\xi = -1/6$ is allowed by constraints from *Planck* 2018, BAO and H_0 measurements.

Constraints from *Planck* 2018 TT+TE+EE + CMB Lensing,
BAO + EFT and SH0ES

Parameter	Λ CDM	CIMG
$\log(10^{10} A_s)$	$3.051 (3.040)^{+0.014}_{-0.016}$	$3.052 (3.059) \pm 0.015$
n_s	$0.9690 (0.9683) \pm 0.0037$	$0.9721 (0.9751) \pm 0.0041$
$100\theta_s$	$1.04205 (1.04195) \pm 0.00028$	$1.04204 (1.04189) \pm 0.00028$
$100 \times \Omega_b h^2$	$2.252 (2.260) \pm 0.013$	$2.249 (2.247) \pm 0.013$
$\Omega_c h^2$	$0.1182 (0.1184) \pm 0.0009$	$0.1192 (0.1191) \pm 0.0010$
τ_{reio}	$0.0594 (0.0551)^{+0.068}_{-0.082}$	$0.0573 (0.0630)^{+0.0069}_{-0.0078}$
$\phi_i [M_P]$	–	$0.328 (0.353)^{+0.11}_{-0.062}$
$H_0 [\text{km/s/Mpc}]$	$68.21 (68.18) \pm 0.42$	$69.58 (69.67) \pm 0.80$
Ω_m	$0.3039 (0.3048) \pm 0.0055$	$0.2940 (0.2929) \pm 0.0071$
σ_8	$0.8084 (0.8040)^{-0.0063}_{+0.0057}$	$0.8270 (0.8310) \pm 0.011$
S_8	$0.814 (0.810) \pm 0.010$	$0.818 (0.821) \pm 0.011$
$\Delta G_N (\%)$	–	$1.94 (2.08) \pm 0.94$

Table VII. The mean $\pm 1\sigma$ (68% CL) constraints on the cosmological parameters in Λ CDM and CIMG, as inferred from the combination of *Planck* 2018 primary CMB data (TT+TE+EE); *Planck* 2018 CMB lensing data; BAO (BOSS DR12) combined with EFT of BOSS and the latest SH0ES H_0 constraint. This combination of datasets yields the strongest evidence for the CIMG model, as $\phi_i = 0.33^{+0.16}_{-0.20} M_P$ and $\Delta G_N = 1.9 \pm 1.8$ with 95% CL, with $\gtrsim 2\sigma$ significance.

χ^2 statistics from the fit to *Planck* 2018 TT+TE+EE + CMB Lensing, BAO + EFT and SH0ES

Datasets	Λ CDM	CIMG
CMB TT, EE, TE:		
<i>Planck</i> 2018 low- ℓ TT	22.6	22.2
<i>Planck</i> 2018 low- ℓ EE	396.7	398.3
<i>Planck</i> 2018 high- ℓ TT+TE+EE	2356.0	2355.0
LSS:		
<i>Planck</i> CMB lensing	9.2	9.1
BAO+EFT (SGC high z)	62.7	64.2
BAO+EFT (NGC low z)	70.8	71.0
BAO+EFT (NGC high z)	67.1	66.0
SH0ES	16.6	9.4
Total χ^2	3001.7	2995.2

Table VIII. χ^2 values for the best-fit Λ CDM and CIMG models, constrained by CMB + CMB Lensing + BAO + EFT + SH0ES. There is reduction of 6.5 in χ^2 , for the one additional parameter of the CIMG model.

Near future experiments may be able to put stronger constraints on the MG model and either exclude or affirm the CIMG model. Here we consider the planned ground-based CMB ‘Stage-4’ experiment (CMB-S4) [63, 64]. In order to obtain a forecast for CMB-S4 constraints on the MG model we adopt the expected survey performance of

CMB-S4⁶ and employ standard Fisher analysis [65–67]. The CMB power spectra can be written as

$$C_\ell^{XY} = (4\pi)^2 \int dk k^2 \mathcal{T}_\ell^X(k) \mathcal{T}_\ell^Y(k) P_\zeta(k), \quad (10)$$

where $X, Y = \{T, E\}$ stand for temperature and E-mode polarization, and \mathcal{T}_ℓ^X are their transfer functions.

The forecast on the variance for a set of parameters θ_i may be obtained by defining the Fisher matrix as

$$F_{ij} = \sum_\ell \frac{2\ell+1}{2} f_{\text{sky}} \text{Tr} \left[C_\ell^{-1} \frac{\partial C_\ell}{\partial \theta_i} C_\ell^{-1} \frac{\partial C_\ell}{\partial \theta_j} \right], \quad (11)$$

where f_{sky} is the sky-fraction covered and C_ℓ are the covariance matrices, which are given by

$$C_\ell = \begin{pmatrix} \tilde{C}_\ell^{TT} & \tilde{C}_\ell^{TE} & \tilde{C}_\ell^{Td} \\ \tilde{C}_\ell^{TE} & \tilde{C}_\ell^{EE} & \tilde{C}_\ell^{Ed} \\ \tilde{C}_\ell^{Td} & \tilde{C}_\ell^{Ed} & \tilde{C}_\ell^{dd} \end{pmatrix}, \quad (12)$$

where we have defined

$$\tilde{C}_\ell^{XY} \equiv C_\ell^{XY} + N_\ell^{XY}, \quad (13)$$

where N_ℓ^{XY} are the noise power spectra, given by

$$\begin{aligned} N_\ell^{TT} &= \Delta_T^2 e^{\ell(\ell+1)\sigma_b^2} \\ N_\ell^{EE} &= 2 \times N_\ell^{TT}, \end{aligned} \quad (14)$$

⁶ CMB-S4 performance expectations: https://cmb-s4.org/wiki/index.php/Survey_Performance_Expectations

Forecast on constraints on cosmological parameters in MG scenario from CMB-S4

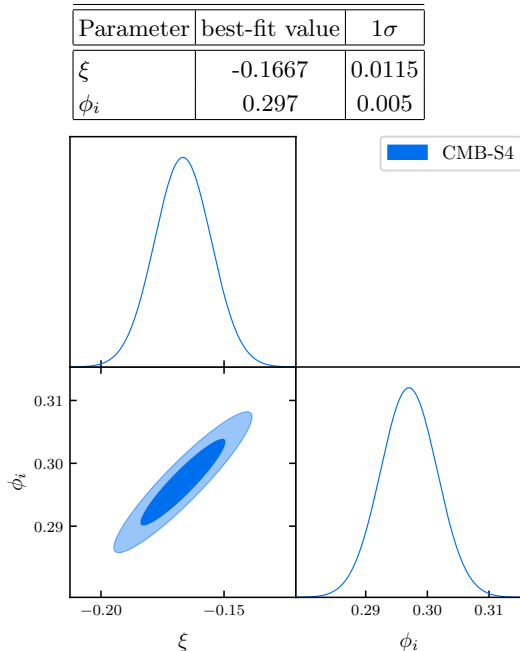


Figure 3. Constraints on modified gravity (MG) parameters and H_0 , expected by the planned CMB-S4 experiment, after maximizing over all the cosmological parameters. We can expect CMB-S4 constraints on MG parameters to be at least an order of magnitude smaller than the values themselves, thus advocating whether the CI scenario is favorable or not.

where Δ_T is the temperature sensitivity, $\sigma_b = \theta_{\text{FWHM}}/\sqrt{8 \log 2}$, with the full-width-half-maximum θ_{FWHM} given in radians. For the lensing noise N_{ell}^{dd} we follow Ref. [68], constructing it from the E and B modes data, then subtracting from the B-mode data which is in turn used again to construct N_{ell}^{dd} and so forth, until we reach convergence. We use the 93, 145 and 225 GHz frequencies, with the corresponding sensitivities of $\Delta T = 1.5, 1.5, 4.8 \mu\text{K-arcmin}$, resolution of $\theta_{\text{FWHM}} = 2.2, 1.4, 1.0 \text{ arcmin}$, over 40% of the sky and a prior on the optical depth of reionization of $\tau = 0.06 \pm 0.01$. The CMB-S4 experiment is expected to observe the ℓ range between 30 and 5000 for polarization, although the highest modes will be noise-dominated. We also ignore $\ell > 3000$ for temperature, as higher multipoles would be contaminated by foregrounds.

Finally we define the correlation matrix as $C_{ij} \equiv F_{ij}^{-1}$, thus the variance of each of the parameters Θ_i is $\sigma = \sqrt{C_{ii}}$. For the fiducial values of the parameters we use the best fit values in Table III. The expected constraints on MG parameters from CMB-S4 experiment are shown in Table 3. We find that the CMB-S4 experiment is expected to place strong constraints on ξ and can help determine if CI scenario is preferred. We can also expect CMB-S4 to improve constraints from *Planck* on the evidence for physics beyond ΛCDM (e.g. EDE, CIMG).

VI. DISCUSSION AND CONCLUSIONS

In recent years the discrepancy between the values of the Hubble constant H_0 , the current expansion rate of the Universe, inferred from early-Universe measurements, such as *Planck* 2018 CMB, and late-Universe measurements, such as the SH0ES collaboration distance-ladder measurements, has reached $\gtrsim 4\sigma$ confidence.

A recent review, Ref. [5], of the phenomenology of the Hubble tension suggests that, to restore concordance between recent cosmological data and the cosmological model, increasing the value of H_0 alone is not enough, but one should reduce the value of the sound horizon at last scattering r_s^* as well. It was also suggested that the most promising method to accomplish this goal is by introducing new physics just prior to recombination, at the proximity of matter-radiation equality, which would trigger a rapid increase of the expansion rate throughout this period. A typical way of realizing this methodology is to introduce a new energy component to the cosmological model, so that it will increase $H(z)$ throughout this period and then dilute fast enough to be negligible at later epochs.

In this work we considered the CIMG model as a candidate for alleviating the Hubble tension. We analyzed it using various combinations of datasets composed of early-Universe data, direct measurements of H_0 and LSS data: *Planck* 2018 CMB and its lensing, BAO (6dF, SDSS DR7 and SDSS DR12), SDSS DR12 RSD, SN distance data from Pantheon, SH0ES distance-ladder measurements of H_0 , DES-Y1 3x2pt and BAO+EFT (BOSS/SDSS galaxies clustering DR12). We also compared the results to a similar analysis done for the EDE model [7]. The constraints we found on the CIMG model and its influence on other cosmological parameters share many of the characteristics of the EDE model, while the former introduces only one additional parameter to the cosmological model and is not fine tuned as the latter, which requires at least two additional parameters. We find that the CIMG model allows an increase of the Hubble parameter up to $H_0 = 69.58 \pm 0.80 \text{ km/s/Mpc}$, when considering all types of datasets (summarized results in Table IX and Fig. 4).

Initially we considered primary CMB anisotropies alone: *Planck* 2018 TT+TE+EE. Although the value of H_0 is increased slightly, there is no significant evidence for the CIMG model (Table I). Furthermore, the total fit to the CMB is worsened in the CIMG scenario, compared to ΛCDM . We conclude that the CIMG model is not preferred by primary CMB data alone. In contrast to the EDE scenario, in which the posterior of the EDE component might be biased due to degeneracy of the other parameters of the model (as describe in Ref. [10]), the posterior of ϕ_i , shown in Fig. 4, indicates accurately the preference of the dataset. For the P18 dataset it is located around zero, indicating it disfavors CIMG.

When we supplement the primary CMB dataset with *Planck* 2018 lensing + BAO + RSD + SNIa + SH0ES, we find, as shown in Table III, a substantial CIMG

Constraints summary on CIMG for varying data sets

Parameter	<i>Planck</i> 2018 TT+TE+EE	<i>Planck</i> 2018 TT+TE+EE, CMB lensing, BAO, RSD, SNIa and SH0ES	<i>Planck</i> 2018 TT+TE+EE, CMB lensing, BAO, RSD, SNIa, SH0ES and DES-Y1	<i>Planck</i> 2018 TT+TE+EE, CMB lensing, BAO+EFT and SH0ES
$\phi_i [M_P]$	< 0.213	$0.297^{+0.11}_{-0.075}$	$0.264^{+0.13}_{-0.072}$	$0.328^{+0.11}_{-0.062}$
$\Delta G_N (\%)$	$0.68^{+0.14}_{-0.75}$	$1.70^{+0.81}_{-1.1}$	$1.36^{+0.68}_{-1.1}$	1.94 ± 0.94
$H_0 [\text{km/s/Mpc}]$	$67.98^{+0.63}_{-1.1}$	$69.24^{+0.60}_{-0.83}$	$69.40^{+0.60}_{-0.75}$	69.58 ± 0.80
σ_8	$0.8170^{+0.022}_{-0.020}$	$0.8242^{+0.0090}_{-0.012}$	$0.8176^{+0.0087}_{-0.0110}$	0.8270 ± 0.011
S_8	0.830 ± 0.016	0.820 ± 0.010	0.809 ± 0.009	0.818 ± 0.011
$\Delta\chi^2$	+4.8	-9	-0.8	-6.5

Table IX. The mean $\pm 1\sigma$ constraints on cosmological parameters in the CIMG scenario from *Planck* 2018; CMB lensing; BAO; SNIa; SH0ES; RSD; DES-Y1; and a combined BAO+EFT dataset. Only ϕ_i is a sampled parameter. The significance of the CIMG component is highly dependent on the datasets: the inclusion of SH0ES tends to increase the value of ϕ_i , whereas the inclusion of DES-Y1 reduces its value. The right column refers to another dataset composed of the BAO+EFT likelihood, which allows for a larger value for ϕ_i . Even the highest value found for H_0 does not relieve the Hubble tension completely.

Constraints on CIMG parameter from varying sets of data

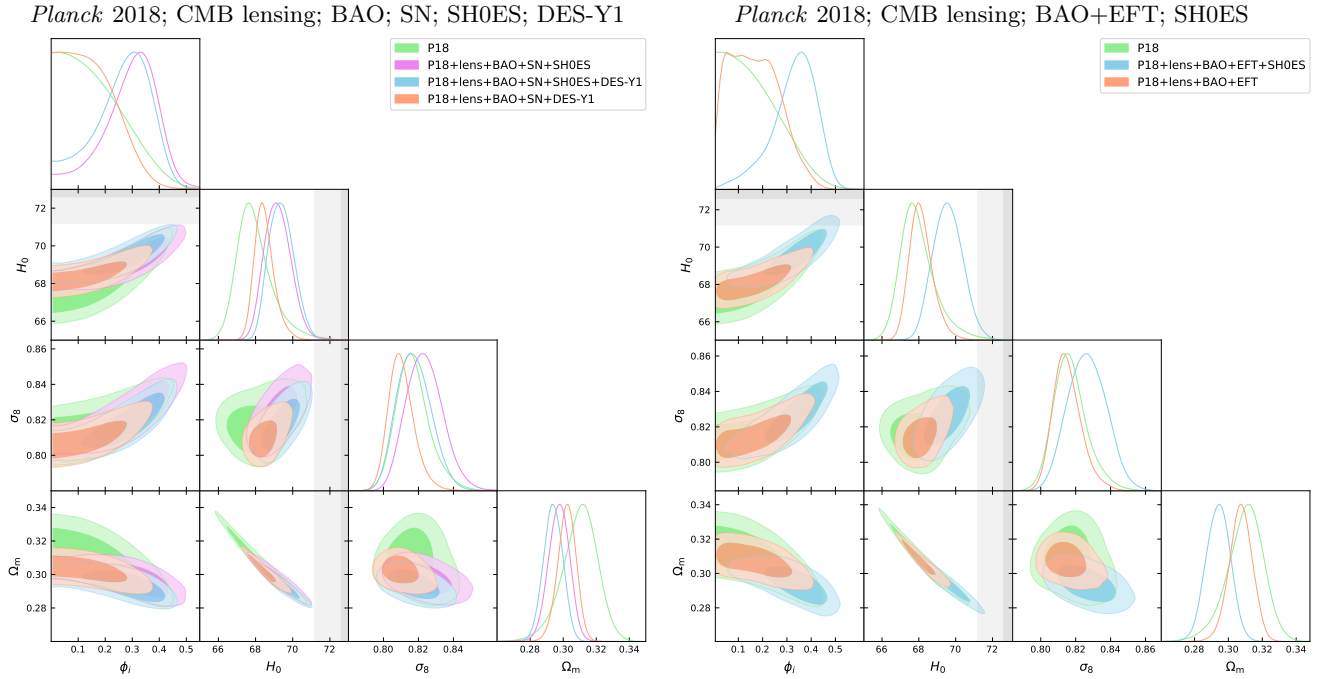


Figure 4. Constraints on the CIMG parameter from various datasets: primary *Planck* 2018; CMB lensing; BAO; RSD; SNIa; SH0ES; DES-Y1; and a combined BAO+EFT. Here we present a subset of the parameters: the initial condition ϕ_i for the CIMG, along with H_0 [km/s/Mpc] and σ_8 . The contours show 1σ and 2σ posteriors for various dataset combinations, computed with GetDist [50]. The P18 dataset alone (green) yields a posterior for ϕ_i which tends to zero, thus disfavoring a significant CIMG component, in contrast to the combined datasets (purple and blue), which feature a significant CIMG component. The EFT dataset seems to put lower constraints on σ_8 than DES-Y1, as shown in its posteriors for each dataset, which explains the more significant CIMG component when using the EFT instead of DES-Y1 (blue on each side). Here we also include datasets without SH0ES (salmon), in which the CIMG significance is almost completely erased, indicating the low preference of the model by all other datasets.

component, corresponding to $\phi_i = 0.3^{+0.14}_{-0.24} M_P$ and $H_0 = 69.24 \pm 1.4$ km/s/Mpc at %95 CL. The tension

with the SH0ES measurements is reduced to 3.1σ , while the tension with LSS data, 2.4σ , is only slightly greater

than that of the Λ CDM benchmark. The CIMG model offers a better fit to this combined dataset as $\Delta\chi^2 = -9$. This reduction of $\Delta\chi^2$ is mainly due to the better fit to SH0ES data, as shown in Table IV. We note that the better fit to both CMB and SH0ES data comes at the expense of a worse fit to BAO and lensing data (the LSS part of this dataset), indicating a correlation between the different datasets. As described in Ref. [7] for the EDE model, the introduction of the CIMG component forces some cosmological parameters to shift in order to keep the fit to the CMB data. But, due to the increase in the gravitational strength and the non-localized dynamics of the CIMG model, the shifts in $\Omega_c h^2$ and n_s are very small compared to the EDE model. However, for the same reason, the downward shift in Ω_m is more significant, suppressing the increase in S_8 due to the increase in the matter clustering amplitude σ_8 . The correlation between the cosmological parameters is shown in Fig. 2.

Including the DES-Y1 likelihood in the combined dataset, we saw that the posterior of ϕ_i is driven slightly backwards (Fig. 4), corresponding to a smaller CIMG component. The inclusion of DES-Y1 likelihood acts to reduce the value of S_8 , due to the stronger constraints on Ω_m , resulting in smaller tension with the LSS data. Nevertheless, the fit to LSS datasets is worse than that of the Λ CDM benchmark, as the fit to BAO+RSD (BOSS DR12) dataset worsens compared to the improvement exhibited by the benchmark, as shown in Table VI. Excluding SH0ES from the combined dataset erases the CIMG component, as shown in Fig. 4. These results affirm the correlation between the datasets, which leads to the conclusion that it is not possible to reconcile DES, BAO and SH0ES datasets simultaneously, using the methodology of reducing r_s^* , as recently elaborated in Ref. [6].

We also considered a combined dataset which includes the newly published BAO+EFT likelihood. We found a larger CIMG component than in any other combination

of datasets, $\phi_i = 0.33^{+0.16}_{-0.20} M_P$ at %95 CL, which corresponds to $H_0 = 69 \pm 1.6$ km/s/Mpc. The relatively large CIMG component is followed by a large value for σ_8 , but due to the significant reduction in Ω_m (Table VII), which is allowed by this dataset, the resulting value of S_8 is not increased as one would have expected (compared to the values in Table III, for example). Excluding SH0ES from this dataset also results in significant decrease of the CIMG component, however not to the same extent as in the datasets with DES, as shown in Fig. 4.

Finally, forecasts for the near-future ground experiment CMB-S4 show that we can expect it to place strong constraints on the parameter ξ to distinguish the CIMG model from the more general MG, and also to place stronger constraints on ϕ_i . In light of the results of our analysis, the CIMG model might present a rather elegant and natural solution to relieve the Hubble tension, compared to EDE, but since no model that acts to increase H_0 by reducing r_s^* seems to be able to reconcile BAO, DES and SH0ES at the same time, the search for new physics to explain the Hubble tension has not concluded.

Note added: While this paper was undergoing the last round of text edits, Ref. [69] appeared on the arXiv with overall consistent conclusions in its short discussion of the model analyzed in depth here.

ACKNOWLEDGMENTS

We thank Sunny Itzhaki and Marc Kamionkowski for useful discussions and Tristan Smith, Mikhail Ivanov, Miguel Zumalacarregui and especially Colin Hill and José Luis Bernal for tremendous help with the modified CMB codes and the implementation of the various likelihoods in our MCMC analyses. EDK is supported by a faculty fellowship from the Azrieli Foundation.

-
- [1] A. Sandage, G. Tammann, A. Saha, B. Reindl, F. Macchetto, and N. Panagia, *Astrophys. J.* **653**, 843 (2006), [arXiv:astro-ph/0603647](#).
 - [2] A. G. Riess, S. Casertano, W. Yuan, L. M. Macri, and D. Scolnic, *Astrophys. J.* **876**, 85 (2019), [arXiv:1903.07603 \[astro-ph.CO\]](#).
 - [3] N. Aghanim *et al.* (Planck), (2018), [arXiv:1807.06209 \[astro-ph.CO\]](#).
 - [4] L. Verde, T. Treu, and A. Riess (2019) [arXiv:1907.10625 \[astro-ph.CO\]](#).
 - [5] L. Knox and M. Millea, *Phys. Rev. D* **101**, 043533 (2020), [arXiv:1908.03663 \[astro-ph.CO\]](#).
 - [6] K. Jedamzik, L. Pogosian, and G.-B. Zhao, (2020), [arXiv:2010.04158 \[astro-ph.CO\]](#).
 - [7] J. C. Hill, E. McDonough, M. W. Toomey, and S. Alexander, *Phys. Rev. D* **102**, 043507 (2020), [arXiv:2003.07355 \[astro-ph.CO\]](#).
 - [8] M. M. Ivanov, E. McDonough, J. C. Hill, M. Simonović, M. W. Toomey, S. Alexander, and M. Zaldarriaga, *Phys. Rev. D* **102**, 103502 (2020), [arXiv:2006.11235 \[astro-ph.CO\]](#).
 - [9] G. D'Amico, L. Senatore, and P. Zhang, (2020), [arXiv:2003.07956 \[astro-ph.CO\]](#).
 - [10] T. L. Smith, V. Poulin, J. L. Bernal, K. K. Boddy, M. Kamionkowski, and R. Murgia, (2020), [arXiv:2009.10740 \[astro-ph.CO\]](#).
 - [11] M.-X. Lin, W. Hu, and M. Raveri, (2020), [arXiv:2009.08974 \[astro-ph.CO\]](#).
 - [12] V. Poulin, T. L. Smith, D. Grin, T. Karwal, and M. Kamionkowski, *Phys. Rev. D* **98**, 083525 (2018), [arXiv:1806.10608 \[astro-ph.CO\]](#).
 - [13] T. L. Smith, V. Poulin, and M. A. Amin, *Phys. Rev. D* **101**, 063523 (2020), [arXiv:1908.06995 \[astro-ph.CO\]](#).
 - [14] P. Agrawal, F.-Y. Cyr-Racine, D. Pinner, and L. Randall, (2019), [arXiv:1904.01016 \[astro-ph.CO\]](#).
 - [15] S. Alexander and E. McDonough, *Phys. Lett. B* **797**, 134830 (2019), [arXiv:1904.08912 \[astro-ph.CO\]](#).

- [16] M.-X. Lin, G. Benevento, W. Hu, and M. Raveri, *Phys. Rev. D* **100**, 063542 (2019), [arXiv:1905.12618 \[astro-ph.CO\]](#).
- [17] J. Sakstein and M. Trodden, *Phys. Rev. Lett.* **124**, 161301 (2020), [arXiv:1911.11760 \[astro-ph.CO\]](#).
- [18] F. Niedermann and M. S. Sloth, (2019), [arXiv:1910.10739 \[astro-ph.CO\]](#).
- [19] N. Kaloper, *Int. J. Mod. Phys. D* **28**, 1944017 (2019), [arXiv:1903.11676 \[hep-th\]](#).
- [20] K. V. Berghaus and T. Karwal, *Phys. Rev. D* **101**, 083537 (2020), [arXiv:1911.06281 \[astro-ph.CO\]](#).
- [21] M. Braglia, M. Ballardini, W. T. Emond, F. Finelli, A. E. Gumrukcuoglu, K. Koyama, and D. Paoletti, *Phys. Rev. D* **102**, 023529 (2020), [arXiv:2004.11161 \[astro-ph.CO\]](#).
- [22] G. Ballesteros, A. Notari, and F. Rompineve, (2020), [arXiv:2004.05049 \[astro-ph.CO\]](#).
- [23] M. Ballardini, M. Braglia, F. Finelli, D. Paoletti, A. A. Starobinsky, and C. Umiltà, (2020), [arXiv:2004.14349 \[astro-ph.CO\]](#).
- [24] M. Zumalacárregui, *Phys. Rev. D* **102**, 023523 (2020), [arXiv:2003.06396 \[astro-ph.CO\]](#).
- [25] S. Joudaki *et al.*, *Astron. Astrophys.* **638**, L1 (2020), [arXiv:1906.09262 \[astro-ph.CO\]](#).
- [26] T. Abbott *et al.* (DES), *Phys. Rev. D* **98**, 043526 (2018), [arXiv:1708.01530 \[astro-ph.CO\]](#).
- [27] H. Hildebrandt *et al.*, *Mon. Not. Roy. Astron. Soc.* **465**, 1454 (2017), [arXiv:1606.05338 \[astro-ph.CO\]](#).
- [28] H. Hildebrandt *et al.*, *Astron. Astrophys.* **633**, A69 (2020), [arXiv:1812.06076 \[astro-ph.CO\]](#).
- [29] C. Hikage *et al.* (HSC), *Publ. Astron. Soc. Jap.* **71**, Publications of the Astronomical Society of Japan, Volume 71, Issue 2, April 2019, 43, <https://doi.org/10.1093/pasj/psz010> (2019), [arXiv:1809.09148 \[astro-ph.CO\]](#).
- [30] M. Rossi, M. Ballardini, M. Braglia, F. Finelli, D. Paoletti, A. A. Starobinsky, and C. Umiltà, *Phys. Rev. D* **100**, 103524 (2019), [arXiv:1906.10218 \[astro-ph.CO\]](#).
- [31] C. Umiltà, M. Ballardini, F. Finelli, and D. Paoletti, *JCAP* **08**, 017 (2015), [arXiv:1507.00718 \[astro-ph.CO\]](#).
- [32] E. N. Saridakis and M. Tsoukalas, *JCAP* **04**, 017 (2016), [arXiv:1602.06890 \[gr-qc\]](#).
- [33] B. Boisseau, G. Esposito-Farese, D. Polarski, and A. A. Starobinsky, *Phys. Rev. Lett.* **85**, 2236 (2000), [arXiv:gr-qc/0001066](#).
- [34] B. Bertotti, L. Iess, and P. Tortora, *Nature* **425**, 374 (2003).
- [35] C. M. Will, *Living Rev. Rel.* **17**, 4 (2014), [arXiv:1403.7377 \[gr-qc\]](#).
- [36] J. Alvey, N. Sabti, M. Escudero, and M. Fairbairn, *Eur. Phys. J. C* **80**, 148 (2020), [arXiv:1910.10730 \[astro-ph.CO\]](#).
- [37] K. Wang and L. Chen, *Eur. Phys. J. C* **80**, 570 (2020), [arXiv:2004.13976 \[astro-ph.CO\]](#).
- [38] M. Zumalacárregui, E. Bellini, I. Sawicki, J. Lesgourgues, and P. G. Ferreira, *JCAP* **08**, 019 (2017), [arXiv:1605.06102 \[astro-ph.CO\]](#).
- [39] E. Bellini, I. Sawicki, and M. Zumalacárregui, *JCAP* **02**, 008 (2020), [arXiv:1909.01828 \[astro-ph.CO\]](#).
- [40] J. Lesgourgues, (2011), [arXiv:1104.2932 \[astro-ph.IM\]](#).
- [41] D. Blas, J. Lesgourgues, and T. Tram, *JCAP* **07**, 034 (2011), [arXiv:1104.2933 \[astro-ph.CO\]](#).
- [42] J. C. Hill, E. McDonough, and M. W. Toomey, *Class-e* (2020).
- [43] A. Lewis and S. Bridle, *Phys. Rev. D* **66**, 103511 (2002), [arXiv:astro-ph/0205436](#).
- [44] A. Lewis, *Phys. Rev. D* **87**, 103529 (2013), [arXiv:1304.4473 \[astro-ph.CO\]](#).
- [45] R. M. Neal, (2005), [arXiv:math/0502099 \[math.ST\]](#).
- [46] J. Torrado and A. Lewis, (2020), [arXiv:2005.05290 \[astro-ph.IM\]](#).
- [47] A. Gelman and D. B. Rubin, *Statist. Sci.* **7**, 457 (1992).
- [48] B. Audren, J. Lesgourgues, K. Benabed, and S. Prunet, *JCAP* **1302**, 001 (2013), [arXiv:1210.7183 \[astro-ph.CO\]](#).
- [49] T. Brinckmann and J. Lesgourgues, (2018), [arXiv:1804.07261 \[astro-ph.CO\]](#).
- [50] A. Lewis, (2019), [arXiv:1910.13970 \[astro-ph.IM\]](#).
- [51] S. Alam *et al.* (BOSS), *Mon. Not. Roy. Astron. Soc.* **470**, 2617 (2017), [arXiv:1607.03155 \[astro-ph.CO\]](#).
- [52] A. J. Ross, L. Samushia, C. Howlett, W. J. Percival, A. Burden, and M. Manera, *Mon. Not. Roy. Astron. Soc.* **449**, 835 (2015), [arXiv:1409.3242 \[astro-ph.CO\]](#).
- [53] F. Beutler, C. Blake, M. Colless, D. Jones, L. Staveley-Smith, L. Campbell, Q. Parker, W. Saunders, and F. Watson, *Mon. Not. Roy. Astron. Soc.* **416**, 3017 (2011), [arXiv:1106.3366 \[astro-ph.CO\]](#).
- [54] N. Kaiser, *Mon. Not. Roy. Astron. Soc.* **227**, 1 (1987).
- [55] S. Satpathy *et al.* (BOSS), *Mon. Not. Roy. Astron. Soc.* **469**, 1369 (2017), [arXiv:1607.03148 \[astro-ph.CO\]](#).
- [56] D. Scolnic *et al.*, *Astrophys. J.* **859**, 101 (2018), [arXiv:1710.00845 \[astro-ph.CO\]](#).
- [57] T. M. C. Abbott, F. B. Abdalla, *et al.*, *MNRAS* **480**, 3879 (2018), [arXiv:1711.00403 \[astro-ph.CO\]](#).
- [58] A. Perko, L. Senatore, E. Jennings, and R. H. Wechsler, (2016), [arXiv:1610.09321 \[astro-ph.CO\]](#).
- [59] G. D’Amico, J. Gleyzes, N. Kokron, K. Markovic, L. Senatore, P. Zhang, F. Beutler, and H. Gil-Marín, *JCAP* **05**, 005 (2020), [arXiv:1909.05271 \[astro-ph.CO\]](#).
- [60] T. Colas, G. D’Amico, L. Senatore, P. Zhang, and F. Beutler, *JCAP* **06**, 001 (2020), [arXiv:1909.07951 \[astro-ph.CO\]](#).
- [61] H. Gil-Marín *et al.*, *Mon. Not. Roy. Astron. Soc.* **460**, 4188 (2016), [arXiv:1509.06386 \[astro-ph.CO\]](#).
- [62] H. Gil-Marín *et al.*, *Mon. Not. Roy. Astron. Soc.* **460**, 4210 (2016), [arXiv:1509.06373 \[astro-ph.CO\]](#).
- [63] K. Abazajian *et al.*, (2019), [arXiv:1907.04473 \[astro-ph.IM\]](#).
- [64] K. N. Abazajian *et al.* (CMB-S4), (2016), [arXiv:1610.02743 \[astro-ph.CO\]](#).
- [65] G. Jungman, M. Kamionkowski, A. Kosowsky, and D. N. Spergel, *Phys. Rev. Lett.* **76**, 1007 (1996), [arXiv:astro-ph/9507080](#).
- [66] G. Jungman, M. Kamionkowski, A. Kosowsky, and D. N. Spergel, *Phys. Rev. D* **54**, 1332 (1996), [arXiv:astro-ph/9512139](#).
- [67] W. Wu, J. Errard, C. Dvorkin, C. Kuo, A. Lee, P. McDonald, A. Slosar, and O. Zahn, *Astrophys. J.* **788**, 138 (2014), [arXiv:1402.4108 \[astro-ph.CO\]](#).
- [68] K. M. Smith, D. Hanson, M. LoVerde, C. M. Hirata, and O. Zahn, *JCAP* **06**, 014 (2012), [arXiv:1010.0048 \[astro-ph.CO\]](#).
- [69] M. Braglia, M. Ballardini, F. Finelli, and K. Koyama, “Early modified gravity in light of the H_0 tension and LSS data,” (2020), [arXiv:2011.12934 \[astro-ph.CO\]](#).